

Masked World Models for Visual Control

Younggyo Seo^{1,2*} Danijar Hafner^{2,3,4} Hao Liu² Fangchen Liu²

Stephen James² Kimin Lee³ Pieter Abbeel²

¹ KAIST ² UC Berkeley ³ Google Research ⁴ University of Toronto

Abstract: Visual model-based reinforcement learning (RL) has the potential to enable sample-efficient robot learning from visual observations. Yet the current approaches typically train a single model end-to-end for learning both visual representations and dynamics, making it difficult to accurately model the interaction between robots and small objects. In this work, we introduce a visual model-based RL framework that decouples visual representation learning and dynamics learning. Specifically, we train an autoencoder with convolutional layers and vision transformers (ViT) to reconstruct pixels given masked convolutional features, and learn a latent dynamics model that operates on the representations from the autoencoder. Moreover, to encode task-relevant information, we introduce an auxiliary reward prediction objective for the autoencoder. We continually update both autoencoder and dynamics model using online samples collected from environment interaction. We demonstrate that our decoupling approach achieves state-of-the-art performance on a variety of visual robotic tasks from Meta-world and RL Bench, *e.g.*, we achieve 81.7% success rate on 50 visual robotic manipulation tasks from Meta-world, while the baseline achieves 67.9%. Code is available on the project website: <https://sites.google.com/view/mwm-rl>.

1 Introduction

Model-based reinforcement learning (RL) holds the promise of sample-efficient robot learning by learning a world model and leveraging it for planning [1, 2, 3] or generating imaginary states for behavior learning [4, 5]. These approaches have also previously been applied to environments with visual observations, by learning an action-conditional video prediction model [6, 7] or a latent dynamics model that predicts compact representations in an abstract latent space [8, 9]. However, learning world models on environments with complex visual observations, *e.g.*, accurately modeling interactions with small objects, is an open challenge.

We argue that this difficulty comes from the design of current approaches that typically optimize the world model end-to-end for learning both visual representations and dynamics [9, 10]. This imposes a trade-off between learning representations and dynamics that can prevent world models from accurately capturing visual details, making it difficult to predict forward into the future. Another approach is to learn representations and dynamics separately, such as earlier work by Ha and Schmidhuber [11] who train a variational autoencoder (VAE) [12] and a dynamics model on top of the VAE features. However, separately-trained VAE representations may not be amenable to dynamics learning [8, 10] or may not capture task-relevant details [11].

On the other hand, masked autoencoders (MAE) [13] have recently been proposed as an effective and scalable approach to visual representation learning, by training a self-supervised vision transformer (ViT) [14] to reconstruct masked patches. While it motivates us to learn world models on top of MAE representations, we find that MAE often struggles to capture fine-grained details within patches. Because capturing visual details, *e.g.*, object positions, is crucial for solving visual control tasks, it is desirable to develop a representation learning method that captures such details but also achieves the benefits of MAE such as stability, compute-efficiency, and scalability.

In this paper, we present Masked World Models (MWM), a visual model-based RL algorithm that decouples visual representation learning and dynamics learning. The key idea of MWM is to train

*Work done while visiting UC Berkeley. Correspondence to younggyo.seo@kaist.ac.kr.

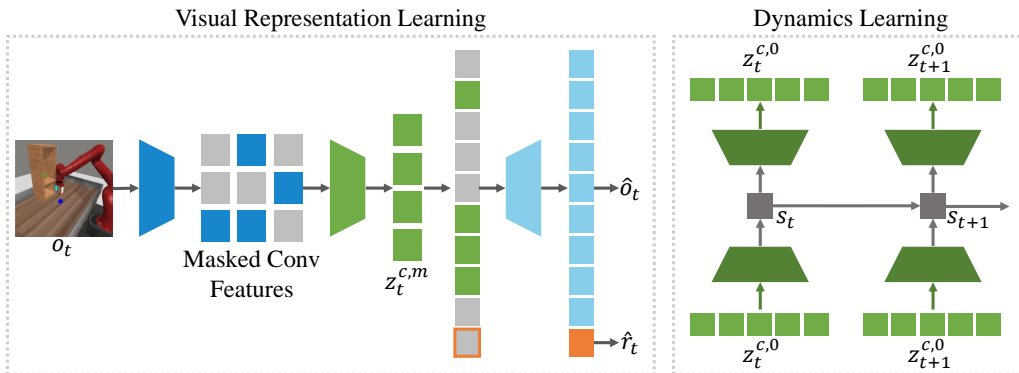


Figure 1: Illustration of our approach. We continually update visual representations and dynamics using online samples collected from environment interaction, by repeating iterative processes of training (Left) an autoencoder with convolutional feature masking and reward prediction and (Right) a latent dynamics model in the latent space of the autoencoder. We note that autoencoder parameters are not updated during dynamics learning.

an autoencoder that reconstructs visual observations with convolutional feature masking, and a latent dynamics model on top of the autoencoder. By introducing early convolutional layers and masking out convolutional features instead of pixel patches, our approach enables the world model to capture fine-grained visual details from complex visual observations. Moreover, in order to learn task-relevant information that might not be captured solely by the reconstruction objective, we introduce an auxiliary reward prediction task for the autoencoder. Specifically, we separately update visual representations and dynamics by repeating the iterative processes of (i) training the autoencoder with convolutional feature masking and reward prediction, and (ii) learning the latent dynamics model that predicts visual representations from the autoencoder (see Figure 1).

Contributions We highlight the contributions of our paper below:

- We demonstrate the effectiveness of decoupling visual representation learning and dynamics learning for visual model-based RL. MWM significantly outperforms a state-of-the-art model-based baseline [15] on various visual control tasks from Meta-world [16] and RLBench [17].
- We show that a self-supervised ViT trained to reconstruct visual observations with convolutional feature masking can be effective for visual model-based RL. Interestingly, we find that masking convolutional features can be more effective than pixel patch masking [13], by allowing for capturing fine-grained details within patches. This is in contrast to the observation in Touvron et al. [18], where both perform similarly on the ImageNet classification task [19].
- We show that an auxiliary reward prediction task can significantly improve performance by encoding task-relevant information into visual representations.

2 Related Work

World models from visual observations There have been several approaches to learn visual representations for model-based approaches via image reconstruction [6, 7, 8, 9, 10, 11, 15, 20, 21, 22], *e.g.*, learning a video prediction model [6, 23] or a latent dynamics model [8, 9, 10]. This has been followed by a series of works that demonstrated the effectiveness of model-based approaches for solving video games [15, 24, 22] and visual robot control tasks [7, 21, 25, 26]. There also have been several works that considered different objectives, including bisimulation [27] and contrastive learning [28, 29, 30]. While most prior works optimize a single model to learn both visual representations and dynamics, we instead develop a framework that decouples visual representation learning and dynamics learning.

Self-supervised vision transformers Self-supervised learning with vision transformers (ViT) [14] has been actively studied. For instance, Chen et al. [31] introduced MoCo-v3 which trains a ViT with contrastive learning. Caron et al. [32] introduced DINO which utilizes a self-distillation loss [33], and demonstrated that self-supervised ViTs contain information about the semantic layout of images.



Figure 2: Examples of visual observations used in our experiments. We consider a variety of visual robot control tasks from Meta-world [16], RLBench [17], and DeepMind Control Suite [41].

Training self-supervised ViTs with masked image modeling [13, 34, 35, 36, 37, 38, 39] has also been successful. In particular, He et al. [13] proposed a masked autoencoder (MAE) that reconstructs masked pixel patches with an asymmetric encoder-decoder architecture. Unlike MAE, we propose to randomly mask features from early convolutional layers [40] instead of pixel patches and demonstrate that self-supervised ViTs can also be effective for visual model-based RL.

We provide more discussion on related works in more detail in [Appendix C](#).

3 Preliminaries

Problem formulation We formulate a visual control task as a partially observable Markov decision process (POMDP) [42], which is defined as a tuple $(\mathcal{O}, \mathcal{A}, p, r, \gamma)$. \mathcal{O} is the observation space, \mathcal{A} is the action space, $p(o_t | o_{<t}, a_{<t})$ is the transition dynamics, r is the reward function that maps previous observations and actions to a reward $r_t = r(o_{\leq t}, a_{<t})$, and $\gamma \in [0, 1)$ is the discount factor.

Dreamer Dreamer [15, 21] is a visual model-based RL method that learns world models from pixels and trains an actor-critic model via latent imagination. Specifically, Dreamer learns a Recurrent State Space Model (RSSM) [9], which consists of following four components:

$$\begin{aligned} \text{Representation model: } s_t &\sim q_\theta(s_t | s_{t-1}, a_{t-1}, o_t) & \text{Image decoder: } \hat{o}_t &\sim p_\theta(\hat{o}_t | s_t) \\ \text{Transition model: } \hat{s}_t &\sim p_\theta(\hat{s}_t | s_{t-1}, a_{t-1}) & \text{Reward predictor: } \hat{r}_t &\sim p_\theta(\hat{r}_t | s_t) \end{aligned} \quad (1)$$

The representation model extracts model state s_t from previous model state s_{t-1} , previous action a_{t-1} , and current observation o_t . The transition model predicts future state \hat{s}_t without the access to current observation o_t . The image decoder reconstructs raw pixels to provide learning signal, and the reward predictor enables us to compute rewards from future model states without decoding future frames. All model parameters θ are trained to jointly learn visual representations and environment dynamics by minimizing the negative variational lower bound [12]:

$$\mathcal{L}(\theta) \doteq \mathbb{E}_{q_\theta(s_{1:T} | a_{1:T}, o_{1:T})} \left[\sum_{t=1}^T \left(-\ln p_\theta(o_t | s_t) - \ln p_\theta(r_t | s_t) + \beta \text{KL}[q_\theta(s_t | s_{t-1}, a_{t-1}, o_t) \| p_\theta(\hat{s}_t | s_{t-1}, a_{t-1})] \right) \right], \quad (2)$$

where β is a hyperparameter that controls the tradeoff between the quality of visual representation learning and the accuracy of dynamics learning [43]. Then, the critic is learned to regress the values computed from imaginary rollouts, and the actor is trained to maximize the values by propagating analytic gradients back through the transition model (see [Appendix A](#) for the details).

Masked autoencoder Masked autoencoder (MAE) [13] is a self-supervised visual representation technique that trains an autoencoder to reconstruct raw pixels with randomly masked patches consisting of pixels. Following a scheme introduced in vision transformer (ViT) [14], the observation $o_t \in \mathbb{R}^{H \times W \times C}$ is processed with a patchify stem that reshapes o_t into a sequence of 2D patches $h_t \in \mathbb{R}^{N \times (P^2 C)}$, where P is the patch size and $N = HW/P^2$ is the number of patches. Then a subset of patches is randomly masked with a ratio of m to construct $h_t^m \in \mathbb{R}^{M \times (P^2 C)}$.

$$\text{Patchify stem: } h_t = f_\phi^{\text{patch}}(o_t) \quad \text{Masking: } h_t^m \sim p^{\text{mask}}(h_t^m | h_t, m) \quad (3)$$

A ViT encoder embeds only the remaining patches h_t^m into D -dimensional vectors, concatenates the embedded tokens with a learnable CLS token, and processes them through a series of Transformer layers [44]. Finally, a ViT decoder reconstructs the observation by processing tokens from the encoder and learnable mask tokens through Transformer layers followed by a linear output head:

$$\text{ViT encoder: } z_t^m \sim p_\phi(z_t^m | h_t^m) \quad \text{ViT decoder: } \hat{o}_t \sim p_\phi(\hat{o}_t | z_t^m) \quad (4)$$

All the components parameterized by ϕ are jointly optimized to minimize the mean squared error (MSE) between the reconstructed and original pixel patches. MAE computes z_t^0 without masking, and utilizes its first component (*i.e.*, CLS representation) for downstream tasks (*e.g.*, image classification).

4 Masked World Models

In this section, we present Masked World Models (MWM), a visual model-based RL framework for learning accurate world models by separately learning visual representations and environment dynamics. Our method repeats (i) updating an autoencoder with convolutional feature masking and an auxiliary reward prediction task (see Section 4.1), (ii) learning a dynamics model in the latent space of the autoencoder (see Section 4.2), and (iii) collecting samples from environment interaction. We provide the overview and pseudocode of MWM in Figure 1 and Appendix D, respectively.

4.1 Visual Representation Learning

It has been observed that masked image modeling with a ViT architecture [13, 34, 36] enables compute-efficient and stable self-supervised visual representation learning. This motivates us to adopt this approach for visual model-based RL, but we find that masked image modeling with commonly used pixel patch masking [13] often makes it difficult to learn fine-grained details within patches, *e.g.*, small objects (see Appendix B for a motivating example). While one can consider small-size patches, this would increase computational costs due to the quadratic complexity of self-attention layers.

To handle this issue, we instead propose to train an autoencoder that reconstructs raw pixels given randomly masked convolutional features. Unlike previous approaches that utilize a patchify stem and randomly mask pixel patches (see Section 3), we adopt a convolution stem [14, 40] that processes o_t through a series of convolutional layers followed by a flatten layer, to obtain $h_t^c \in \mathbb{R}^{N_c \times D}$ where N_c is the number of convolutional features. Then h_t^c is randomly masked with a ratio of m to obtain $h_t^{c,m} \in \mathbb{R}^{M_c \times D}$, and ViT encoder and decoder process $h_t^{c,m}$ to reconstruct raw pixels.

$$\begin{aligned} \text{Convolution stem: } h_t^c &= f_\phi^{\text{conv}}(o_t) & \text{Masking: } h_t^{c,m} &\sim p^{\text{mask}}(h_t^{c,m} | h_t^c, m) \\ \text{ViT encoder: } z_t^{c,m} &\sim p_\phi(z_t^{c,m} | h_t^{c,m}) & \text{ViT decoder: } \hat{o}_t &\sim p_\phi(\hat{o}_t | z_t^{c,m}) \end{aligned} \quad (5)$$

Because early convolutional layers mix low-level details, we find that our autoencoder can effectively reconstruct all the details within patches by learning to extract information from nearby non-masked features (see Figure 7 for examples). This enables us to learn visual representations capturing such details while also achieving the benefits of MAE, *e.g.*, stability and compute-efficiency.

Reward prediction In order to encode task-relevant information that might not be captured solely by the reconstruction objective, we introduce an auxiliary objective for the autoencoder to predict rewards jointly with pixels. Specifically, we make the autoencoder predict the reward r_t from $z_t^{c,m}$ in conjunction with raw pixels.

$$\text{ViT decoder with reward prediction: } \hat{o}_t, \hat{r}_t \sim p_\phi(\hat{o}_t, \hat{r}_t | z_t^{c,m}) \quad (6)$$

In practice, we concatenate one additional learnable mask token to inputs of the ViT decoder, and utilize the corresponding output representation for predicting the reward with a linear output head.

High masking ratio Introducing early convolutional layers might impede the masked reconstruction tasks because they propagate information across patches [18], and the model can exploit this to find a shortcut to solve reconstruction tasks. However, we find that a high masking ratio (*i.e.*, 75%) can prevent the model from finding such shortcuts and induce useful representations (see Figure 6(b) for supporting experimental results). This also aligns with the observation from Touvron et al. [18], where masked image modeling [34] with a convolution stem [45] can achieve competitive performance with the patchify stem on the ImageNet classification task [19].

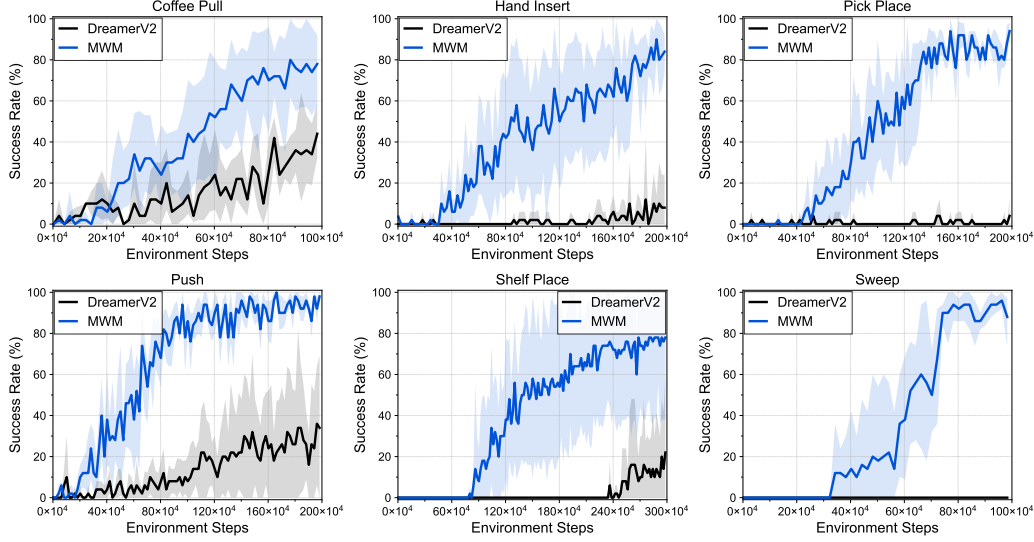


Figure 3: Learning curves on six visual robotic manipulation tasks from Meta-world as measured on the success rate. We select the tasks that require modeling interactions between small objects and robot arms. Learning curves on 50 tasks are available in [Appendix G](#). The solid line and shaded regions represent the mean and bootstrap confidence intervals, respectively, across five runs.

4.2 Latent Dynamics Learning

Once we learn visual representations, we leverage them for efficiently learning a dynamics model in the latent space of the autoencoder. Specifically, we obtain the frozen representations $z_t^{c,0}$ from the autoencoder, and then train a variant of RSSM whose inputs and reconstruction targets are $z_t^{c,0}$, by replacing the representation model and the image decoder in [Equation 1](#) with following components:

$$\begin{aligned} \text{Representation model:} \quad & s_t \sim q_\theta(s_t | s_{t-1}, a_{t-1}, z_t^{c,0}) \\ \text{Visual representation decoder:} \quad & \hat{z}_t^{c,0} \sim p_\theta(\hat{z}_t^{c,0} | s_t) \end{aligned} \quad (7)$$

Because visual representations capture both high- and low-level information in an abstract form, the model can focus more on dynamics learning by reconstructing them instead of raw pixels (see [Section 5.5](#) for relevant discussion). Here, we also note that we utilize all the elements of $z_t^{c,0}$ unlike MAE that only utilizes CLS representation for downstream tasks. We empirically find this enables the model to receive rich learning signals from reconstructing all the representations containing spatial information (see [Appendix I](#) for supporting experiments).

5 Experiments

We evaluate MWM on various robotics benchmarks, including Meta-world [\[16\]](#) (see [Section 5.1](#)), RL Bench [\[17\]](#) (see [Section 5.2](#)), and DeepMind Control Suite [\[46\]](#) (see [Section 5.3](#)). We remark that these benchmarks consist of diverse and challenging visual robotic tasks. We also analyze algorithmic design choices in-depth (see [Section 5.4](#)) and provide a qualitative analysis of how our decoupling approach works by visualizing the predictions from the latent dynamics model (see [Section 5.5](#)).

Implementation We use visual observations of $64 \times 64 \times 3$. For the convolution stem, we stack 3 convolution layers with the kernel size of 4 and stride 2, followed by a linear projection layer. We use a 4-layer ViT encoder and a 3-layer ViT decoder. We find that initializing the autoencoder with a warm-up schedule at the beginning of training is helpful. Unlike MAE, we compute the loss on entire pixels because we do not apply masking to pixels. For world models, we build our implementation on top of DreamerV2 [\[15\]](#). To take a sequence of autoencoder representations as inputs, we replace a CNN encoder and decoder with a 2-layer Transformer encoder and decoder. We use same hyperparameters within the same benchmark. More details are available in [Appendix E](#).

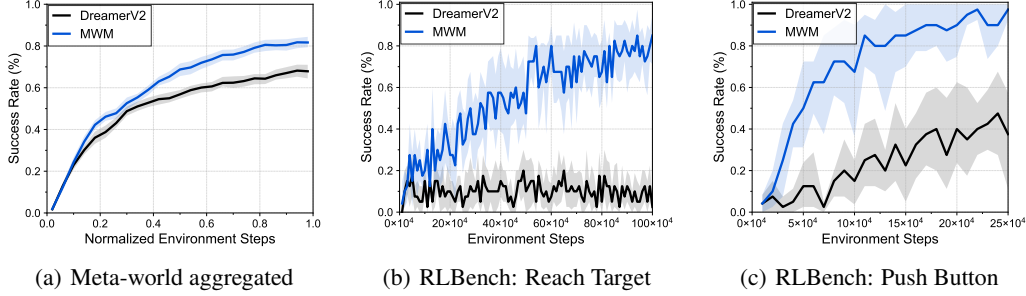


Figure 4: (a) Aggregate performance on all 50 Meta-world tasks. We normalize environment steps by maximum steps in each task. The solid line and shaded regions represent the mean and stratified bootstrap confidence intervals, respectively, across 250 runs. We report the learning curves on (b) Reach Target and (c) Push Button from RL Bench. Performances are not directly comparable to previous results [47, 48] due to the difference in setups (see Section 5.2). The solid line and shaded regions represent the mean and bootstrap confidence intervals, respectively, across eight runs.

5.1 Meta-world Experiments

Environment details In order to use a single camera viewpoint consistently over all 50 tasks, we use the modified corner2 camera viewpoint for all tasks. In our experiments, we classify 50 tasks into easy, medium, hard, and very hard tasks where experiments are run over 500K, 1M, 2M, 3M environments steps with action repeat of 2, respectively. More details are available in Appendix F.

Results In Figure 3, we report the performance on a set of selected six challenging tasks that require agents to control robot arms to interact with small objects. We find that MWM significantly outperforms DreamerV2 in terms of both sample-efficiency and final performance. In particular, MWM achieves $> 80\%$ success rate on Pick Place while DreamerV2 struggles to solve the task. These results show that our approach of separating visual representation learning and dynamics learning can learn accurate world models on challenging domains. Figure 4(a) shows the aggregate performance over all the 50 tasks from the benchmark, demonstrating that our method consistently outperforms DreamerV2 overall. We also provide learning curves on all individual tasks in Appendix G, where MWM consistently achieves similar or better performance on most tasks.

5.2 RL Bench Experiments

Environment details In order to evaluate our method on more challenging visual robotic manipulation tasks, we consider RL Bench [17], which has previously acted as an effective proxy for real-robot performance [48]. Since RL Bench consists of sparse-reward and challenging tasks, solving them typically requires expert demonstrations, specialized network architectures, additional inputs (e.g., point cloud and proprioceptive states), and an action mode that requires path planning [47, 48, 49, 50]. While we could utilize some of these components, we instead leave this as future work in order to maintain a consistent evaluation setup across multiple domains. In our experiments, we instead consider two relatively easy tasks with dense rewards, and utilize an action mode that specifies the delta of joint positions. We provide more details in Appendix F.

Results As shown in Figure 4(b) and Figure 4(c), we observe that our approach can also be effective on RL Bench tasks, significantly outperforming DreamerV2. In particular, DreamerV2 achieves $< 20\%$ success rate on Reach Target, while our approach can solve the tasks with $> 80\%$ success rates. We find that this is because DreamerV2 fails to capture target positions in visual observations, while our method can capture such details (see Section 5.5 for relevant discussion and visualizations). However, we also note that these results are preliminary because they are still too sample-inefficient to be used for real-world scenarios. We provide more discussion in Section 6.

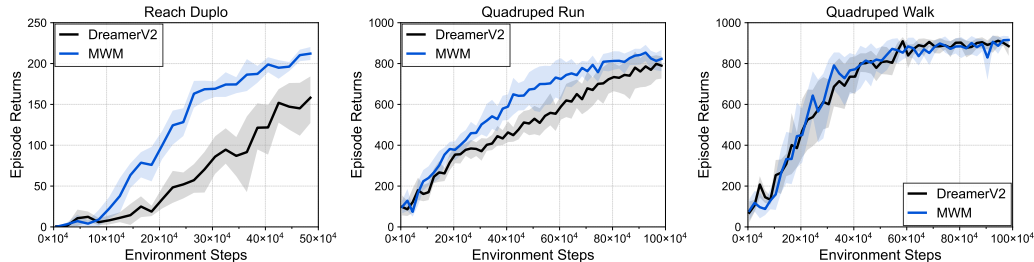


Figure 5: Learning curves on three visual robot control tasks from DeepMind Control Suite as measured on the episode return. The solid line and shaded regions represent the mean and bootstrap confidence intervals, respectively, across eight runs.

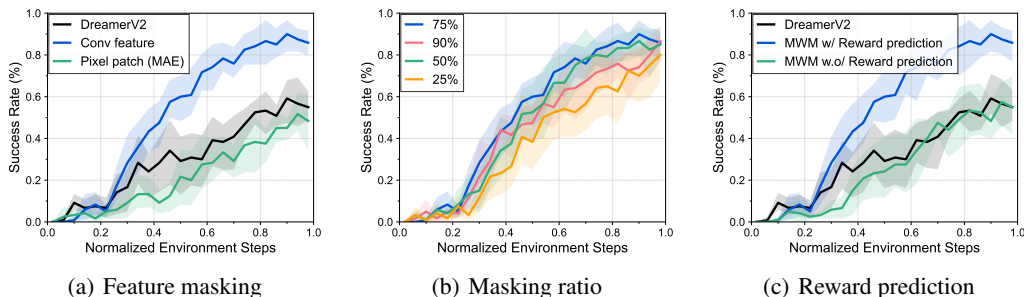


Figure 6: Learning curves on three manipulation tasks from Meta-world that investigate the effect of (a) convolutional feature masking, (b) masking ratio, and (c) reward prediction. The solid line and shaded regions represent the mean and stratified bootstrap confidence interval across 12 runs.

5.3 DeepMind Control Suite Experiments

Environment details In order to demonstrate that our approach is generally applicable to diverse visual control tasks, we also evaluate our method on visual locomotion tasks from the widely used DeepMind Control Suite benchmark. Following a standard setup in Hafner et al. [21], we use an action repeat of 2 and default camera configurations. We provide more details in Appendix F.

Results Figure 5 shows that our method achieves competitive performance to DreamerV2 on visual locomotion tasks (i.e., Quadruped tasks), demonstrating the generality of our approach across diverse visual control tasks. We also observe that our method outperforms DreamerV2 on Reach Duplo, which is one of a few manipulation tasks in the benchmark (see Figure 2(e) for an example). This implies that our method is effective on environments where the model should capture fine-grained details like object positions. More results are available in Appendix H, where trends are similar.

5.4 Ablation Study

Convolutional feature masking We compare convolutional feature masking with pixel masking (i.e., MAE) in Figure 6(a), which shows that convolutional feature masking significantly outperforms pixel masking. This demonstrates that enabling the model to capture fine-grained details within patches can be important for visual control. We also report the performance with varying masking ratio $m \in \{0.25, 0.5, 0.75, 0.9\}$ in Figure 6(b). As we discussed in Section 4.1, we find that $m = 0.75$ achieves better performance than $m \in \{0.25, 0.5\}$ because strong regularization can prevent the model from finding a shortcut from input pixels. However, we also find that too strong regularization (i.e., $m = 0.9$) degrades the performance.

Reward prediction In Figure 6(c), we find that performance significantly degrades without reward prediction, which shows that the reconstruction objective might not be sufficient for learning task-relevant information. It would be an interesting future direction to develop a representation learning scheme that learns task-relevant information without rewards because they might not be available in practice. We provide more ablation studies and learning curves on individual tasks in Appendix I.

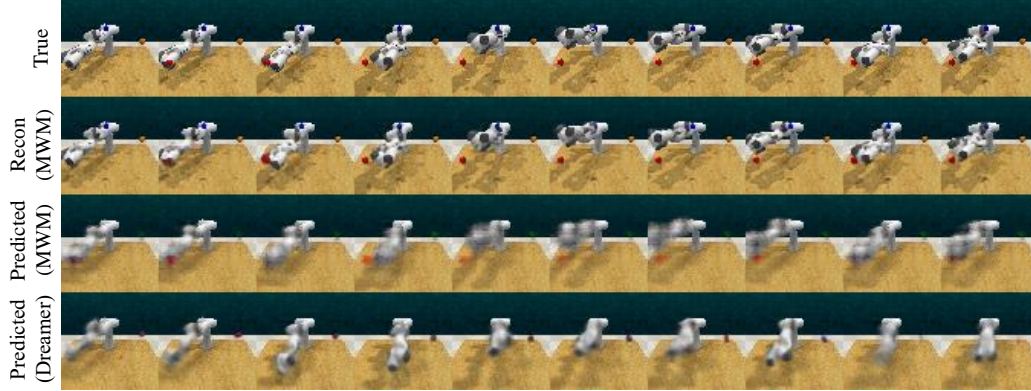


Figure 7: Future frames reconstructed with the autoencoder (*i.e.*, Recon) and predicted by latent dynamics models (*i.e.*, Predicted). Predictions from our model capture the position of a red block, which is a target position a robot arm should reach, but predictions from Dreamer are not capturing such details. In our predictions, the components that are not task-relevant are abstracted away (*i.e.*, blue and orange blocks), though the autoencoder reconstructs them. This shows how our decoupling approach works: it encourages the autoencoder to capture all the details, and the dynamics model to focus on modeling task-relevant components. Best viewed as video provided in [Appendix B](#).

5.5 Qualitative Analysis

We visually investigate how our world model works compared to the world model of DreamerV2. Specifically, we visualize the future frames predicted by latent dynamics models on Reach Target from RLBench in [Figure 7](#). In this task, a robot arm should reach a target position specified by a red block in visual observations (see [Figure 2\(c\)](#)), which changes every trial. Thus it is crucial for the model to accurately predict the position of red blocks for solving the tasks. We find that our world model effectively captures the position of red blocks, while DreamerV2 fails. Interestingly, we also observe that our latent dynamics model ignores the components that are not task-relevant such as blue and orange blocks, though the reconstructions from the autoencoder are capturing all the details. This shows how our decoupling approach works: it encourages the autoencoder to focus on learning representations capturing the details and the dynamics model to focus on modeling task-relevant components of environments. We provide more examples in [Appendix B](#).

6 Discussion

We have presented Masked World Models (MWM), which is a visual model-based RL framework that decouples visual representation learning and dynamics learning. By learning a latent dynamics model operating in the latent space of a self-supervised ViT, we find that our approach allows for solving a variety of visual control tasks from Meta-world, RLBench, and DeepMind Control Suite.

Limitation Despite the results, there are a number of areas for improvement. As we have shown in [Figure 6\(c\)](#), the performance of our approach heavily depends on the auxiliary reward prediction task. This might be because our autoencoder is not learning temporal information, which is crucial for learning task-relevant information. It would be interesting to investigate the performance of video representation learning with ViTs [36, 51]. It would also be interesting to study introducing auxiliary prediction for other modalities, such as audio. Another weakness is that our model operates only on RGB pixels from a single camera viewpoint; we look forward to a future work that incorporates different input modalities such as proprioceptive states and point clouds, building on top of the recent multi-modal learning approaches [52, 53]. Finally, our approach trains behaviors from scratch, which makes it still too sample-inefficient to be used in real-world scenarios. Leveraging a small number of demonstrations, incorporating the action mode with path planning [47], or pre-training a world model on video datasets [54] are directions we hope to investigate in future works.

Acknowledgments

We would like to thank Jongjin Park and Sihyun Yu for helpful discussions. We also thank Cirrascale Cloud Services² for providing compute resources. This work was partially supported by Office of Naval Research under grant N00014-21-1-2769 and grant N00014-22-1-2121, the Darpa RACER program, the Hong Kong Centre for Logistics Robotics, BMW, and Institute of Information & Communications Technology Planning & Evaluation (IITP) grant funded by the Korea government (MSIT) (No.2019-0-00075, Artificial Intelligence Graduate School Program (KAIST)).

References

- [1] K. Chua, R. Calandra, R. McAllister, and S. Levine. Deep reinforcement learning in a handful of trials using probabilistic dynamics models. In *Advances in neural information processing systems*, 2018.
- [2] M. Deisenroth and C. E. Rasmussen. Pilco: A model-based and data-efficient approach to policy search. In *International Conference on Machine Learning*, 2011.
- [3] I. Lenz, R. A. Knepper, and A. Saxena. Deepmpc: Learning deep latent features for model predictive control. In *Robotics: Science and Systems*, 2015.
- [4] T. Kurutach, I. Clavera, Y. Duan, A. Tamar, and P. Abbeel. Model-ensemble trust-region policy optimization. In *International Conference on Learning Representations*, 2018.
- [5] M. Janner, J. Fu, M. Zhang, and S. Levine. When to trust your model: Model-based policy optimization. *Advances in Neural Information Processing Systems*, 2019.
- [6] C. Finn and S. Levine. Deep visual foresight for planning robot motion. In *2017 IEEE International Conference on Robotics and Automation (ICRA)*, 2017.
- [7] F. Ebert, C. Finn, S. Dasari, A. Xie, A. Lee, and S. Levine. Visual foresight: Model-based deep reinforcement learning for vision-based robotic control. *arXiv preprint arXiv:1812.00568*, 2018.
- [8] M. Watter, J. Springenberg, J. Boedecker, and M. Riedmiller. Embed to control: A locally linear latent dynamics model for control from raw images. In *Advances in neural information processing systems*, 2015.
- [9] D. Hafner, T. Lillicrap, I. Fischer, R. Villegas, D. Ha, H. Lee, and J. Davidson. Learning latent dynamics for planning from pixels. In *International Conference on Machine Learning*, 2019.
- [10] M. Zhang, S. Vikram, L. Smith, P. Abbeel, M. Johnson, and S. Levine. Solar: Deep structured representations for model-based reinforcement learning. In *International Conference on Machine Learning*, 2019.
- [11] D. Ha and J. Schmidhuber. World models. In *Advances in Neural Information Processing Systems*, 2018.
- [12] D. P. Kingma and M. Welling. Auto-encoding variational bayes. In *International Conference on Learning Representations*, 2014.
- [13] K. He, X. Chen, S. Xie, Y. Li, P. Dollár, and R. Girshick. Masked autoencoders are scalable vision learners. *arXiv preprint arXiv:2111.06377*, 2021.
- [14] A. Dosovitskiy, L. Beyer, A. Kolesnikov, D. Weissenborn, X. Zhai, T. Unterthiner, M. Dehghani, M. Minderer, G. Heigold, S. Gelly, et al. An image is worth 16x16 words: Transformers for image recognition at scale. In *International Conference on Learning Representations*, 2021.
- [15] D. Hafner, T. Lillicrap, M. Norouzi, and J. Ba. Mastering atari with discrete world models. In *International Conference on Learning Representations*, 2021.

²<https://cirrascale.com>

- [16] T. Yu, D. Quillen, Z. He, R. Julian, K. Hausman, C. Finn, and S. Levine. Meta-world: A benchmark and evaluation for multi-task and meta reinforcement learning. In *Conference on Robot Learning*, 2020.
- [17] S. James, Z. Ma, D. R. Arrojo, and A. J. Davison. RL Bench: The robot learning benchmark & learning environment. *IEEE Robotics and Automation Letters*, 2020.
- [18] H. Touvron, M. Cord, A. El-Nouby, J. Verbeek, and H. Jégou. Three things everyone should know about vision transformers. *arXiv preprint arXiv:2203.09795*, 2022.
- [19] J. Deng, W. Dong, R. Socher, L.-J. Li, K. Li, and L. Fei-Fei. Imagenet: A large-scale hierarchical image database. In *2009 IEEE conference on computer vision and pattern recognition*, 2009.
- [20] C. Finn, X. Y. Tan, Y. Duan, T. Darrell, S. Levine, and P. Abbeel. Deep spatial autoencoders for visuomotor learning. In *2016 IEEE International Conference on Robotics and Automation (ICRA)*, 2016.
- [21] D. Hafner, T. Lillicrap, J. Ba, and M. Norouzi. Dream to control: Learning behaviors by latent imagination. In *International Conference on Learning Representations*, 2020.
- [22] L. Kaiser, M. Babaeizadeh, P. Milos, B. Osinski, R. H. Campbell, K. Czechowski, D. Erhan, C. Finn, P. Kozakowski, S. Levine, et al. Model-based reinforcement learning for atari. In *International Conference on Learning Representations*, 2019.
- [23] A. Gupta, S. Tian, Y. Zhang, J. Wu, R. Martín-Martín, and L. Fei-Fei. Maskvit: Masked visual pre-training for video prediction. *arXiv preprint arXiv:2206.11894*, 2022.
- [24] W. Ye, S. Liu, T. Kurutach, P. Abbeel, and Y. Gao. Mastering atari games with limited data. *Advances in Neural Information Processing Systems*, 2021.
- [25] T. Seyde, W. Schwarting, S. Karaman, and D. Rus. Learning to plan optimistically: Uncertainty-guided deep exploration via latent model ensembles. In *Conference on Robot Learning*, 2021.
- [26] O. Rybkin, C. Zhu, A. Nagabandi, K. Daniilidis, I. Mordatch, and S. Levine. Model-based reinforcement learning via latent-space collocation. In *International Conference on Machine Learning*, 2021.
- [27] C. Gelada, S. Kumar, J. Buckman, O. Nachum, and M. G. Bellemare. Deepmdp: Learning continuous latent space models for representation learning. In *International Conference on Machine Learning*, 2019.
- [28] T. D. Nguyen, R. Shu, T. Pham, H. Bui, and S. Ermon. Temporal predictive coding for model-based planning in latent space. In *International Conference on Machine Learning*, 2021.
- [29] M. Okada and T. Taniguchi. Dreaming: Model-based reinforcement learning by latent imagination without reconstruction. In *2021 IEEE International Conference on Robotics and Automation (ICRA)*, 2021.
- [30] F. Deng, I. Jang, and S. Ahn. Dreamerpro: Reconstruction-free model-based reinforcement learning with prototypical representations. *arXiv preprint arXiv:2110.14565*, 2021.
- [31] X. Chen, S. Xie, and K. He. An empirical study of training self-supervised vision transformers. In *Proceedings of the IEEE/CVF International Conference on Computer Vision*, 2021.
- [32] M. Caron, H. Touvron, I. Misra, H. Jégou, J. Mairal, P. Bojanowski, and A. Joulin. Emerging properties in self-supervised vision transformers. In *Proceedings of the IEEE/CVF International Conference on Computer Vision*, 2021.
- [33] G. Hinton, O. Vinyals, J. Dean, et al. Distilling the knowledge in a neural network. *arXiv preprint arXiv:1503.02531*, 2015.
- [34] H. Bao, L. Dong, and F. Wei. Beit: Bert pre-training of image transformers. *arXiv preprint arXiv:2106.08254*, 2021.

- [35] Z. Li, Z. Chen, F. Yang, W. Li, Y. Zhu, C. Zhao, R. Deng, L. Wu, R. Zhao, M. Tang, et al. Mst: Masked self-supervised transformer for visual representation. In *Advances in Neural Information Processing Systems*, 2021.
- [36] C. Feichtenhofer, H. Fan, Y. Li, and K. He. Masked autoencoders as spatiotemporal learners. *arXiv preprint arXiv:2205.09113*, 2022.
- [37] Z. Xie, Z. Zhang, Y. Cao, Y. Lin, J. Bao, Z. Yao, Q. Dai, and H. Hu. Simmim: A simple framework for masked image modeling. In *Proceedings of the IEEE/CVF Conference on Computer Vision and Pattern Recognition*, 2022.
- [38] C. Wei, H. Fan, S. Xie, C.-Y. Wu, A. Yuille, and C. Feichtenhofer. Masked feature prediction for self-supervised visual pre-training. In *Proceedings of the IEEE/CVF Conference on Computer Vision and Pattern Recognition*, 2022.
- [39] J. Zhou, C. Wei, H. Wang, W. Shen, C. Xie, A. Yuille, and T. Kong. ibot: Image bert pre-training with online tokenizer. *arXiv preprint arXiv:2111.07832*, 2021.
- [40] T. Xiao, M. Singh, E. Mintun, T. Darrell, P. Dollár, and R. Girshick. Early convolutions help transformers see better. In *Advances in Neural Information Processing Systems*, 2021.
- [41] Y. Tassa, S. Tunyasuvunakool, A. Muldal, Y. Doron, S. Liu, S. Bohez, J. Merel, T. Erez, T. Lillicrap, and N. Heess. dm_control: Software and tasks for continuous control. *arXiv preprint arXiv:2006.12983*, 2020.
- [42] R. S. Sutton and A. G. Barto. *Reinforcement learning: An introduction*. MIT Press, 2018.
- [43] A. Alemi, B. Poole, I. Fischer, J. Dillon, R. A. Saurous, and K. Murphy. Fixing a broken elbow. In *International Conference on Machine Learning*, 2018.
- [44] A. Vaswani, N. Shazeer, N. Parmar, J. Uszkoreit, L. Jones, A. N. Gomez, Ł. Kaiser, and I. Polosukhin. Attention is all you need. In *Advances in Neural Information Processing Systems*, 2017.
- [45] B. Graham, A. El-Nouby, H. Touvron, P. Stock, A. Joulin, H. Jégou, and M. Douze. Levit: a vision transformer in convnet’s clothing for faster inference. In *Proceedings of the IEEE/CVF International Conference on Computer Vision*, 2021.
- [46] Y. Tassa, T. Erez, and E. Todorov. Synthesis and stabilization of complex behaviors through online trajectory optimization. In *International Conference on Intelligent Robots and Systems*, 2012.
- [47] S. James and A. J. Davison. Q-attention: Enabling efficient learning for vision-based robotic manipulation. *IEEE Robotics and Automation Letters*, 2022.
- [48] S. James, K. Wada, T. Laidlow, and A. J. Davison. Coarse-to-Fine Q-attention: Efficient learning for visual robotic manipulation via discretisation. *Proceedings of the IEEE/CVF Conference on Computer Vision and Pattern Recognition*, 2022.
- [49] S. James and P. Abbeel. Coarse-to-Fine Q-attention with Learned Path Ranking. *arXiv preprint arXiv:2204.01571*, 2022.
- [50] S. James and P. Abbeel. Coarse-to-Fine Q-attention with Tree Expansion. *arXiv preprint arXiv:2204.12471*, 2022.
- [51] A. Arnab, M. Dehghani, G. Heigold, C. Sun, M. Lučić, and C. Schmid. Vivit: A video vision transformer. In *Proceedings of the IEEE/CVF International Conference on Computer Vision*, 2021.
- [52] X. Geng, H. Liu, L. Lee, D. Schuurams, S. Levine, and P. Abbeel. Multimodal masked autoencoders learn transferable representations. *arXiv preprint arXiv:2205.14204*, 2022.
- [53] R. Bachmann, D. Mizrahi, A. Atanov, and A. Zamir. Multimaes: Multi-modal multi-task masked autoencoders. *arXiv preprint arXiv:2204.01678*, 2022.

- [54] Y. Seo, K. Lee, S. James, and P. Abbeel. Reinforcement learning with action-free pre-training from videos. In *International Conference on Machine Learning*, 2022.
- [55] J. Schulman, P. Moritz, S. Levine, M. Jordan, and P. Abbeel. High-dimensional continuous control using generalized advantage estimation. *arXiv preprint arXiv:1506.02438*, 2015.
- [56] K. He, X. Zhang, S. Ren, and J. Sun. Deep residual learning for image recognition. In *Proceedings of the IEEE conference on computer vision and pattern recognition*, 2016.
- [57] H. Wu, B. Xiao, N. Codella, M. Liu, X. Dai, L. Yuan, and L. Zhang. Cvt: Introducing convolutions to vision transformers. In *Proceedings of the IEEE/CVF International Conference on Computer Vision*, 2021.
- [58] J. Dai, K. He, and J. Sun. Convolutional feature masking for joint object and stuff segmentation. In *Proceedings of the IEEE conference on computer vision and pattern recognition*, pages 3992–4000, 2015.
- [59] J. Tompson, R. Goroshin, A. Jain, Y. LeCun, and C. Bregler. Efficient object localization using convolutional networks. In *Proceedings of the IEEE conference on computer vision and pattern recognition*, 2015.
- [60] G. Ghiasi, T.-Y. Lin, and Q. V. Le. Dropblock: A regularization method for convolutional networks. *Advances in neural information processing systems*, 31, 2018.
- [61] N. Srivastava, G. Hinton, A. Krizhevsky, I. Sutskever, and R. Salakhutdinov. Dropout: a simple way to prevent neural networks from overfitting. *The journal of machine learning research*, 2014.
- [62] J. Park, Y. Seo, C. Liu, L. Zhao, T. Qin, J. Shin, and T.-Y. Liu. Object-aware regularization for addressing causal confusion in imitation learning. In *Advances in Neural Information Processing Systems*, 2021.
- [63] A. Van Den Oord, O. Vinyals, et al. Neural discrete representation learning. In *Advances in Neural Information Processing Systems*, 2017.
- [64] M. Jaderberg, V. Mnih, W. M. Czarnecki, T. Schaul, J. Z. Leibo, D. Silver, and K. Kavukcuoglu. Reinforcement learning with unsupervised auxiliary tasks. In *International Conference on Learning Representations*, 2017.
- [65] M. Schwarzer, A. Anand, R. Goel, R. D. Hjelm, A. Courville, and P. Bachman. Data-efficient reinforcement learning with self-predictive representations. In *International Conference on Learning Representations*, 2021.
- [66] T. Yu, C. Lan, W. Zeng, M. Feng, Z. Zhang, and Z. Chen. Playvirtual: Augmenting cycle-consistent virtual trajectories for reinforcement learning. In *Advances in Neural Information Processing Systems*, 2021.
- [67] T. Yu, Z. Zhang, C. Lan, Z. Chen, and Y. Lu. Mask-based latent reconstruction for reinforcement learning. *arXiv preprint arXiv:2201.12096*, 2022.
- [68] P. S. Castro. Scalable methods for computing state similarity in deterministic markov decision processes. In *Proceedings of the AAAI Conference on Artificial Intelligence*, 2020.
- [69] A. Zhang, R. McAllister, R. Calandra, Y. Gal, and S. Levine. Learning invariant representations for reinforcement learning without reconstruction. In *International Conference on Learning Representations*, 2021.
- [70] A. v. d. Oord, Y. Li, and O. Vinyals. Representation learning with contrastive predictive coding. In *Advances in Neural Information Processing Systems*, 2018.
- [71] A. Anand, E. Racah, S. Ozair, Y. Bengio, M.-A. Côté, and R. D. Hjelm. Unsupervised state representation learning in atari. In *Advances in Neural Information Processing Systems*, 2019.
- [72] B. Mazouze, R. T. d. Combes, T. Doan, P. Bachman, and R. D. Hjelm. Deep reinforcement and infomax learning. In *Advances in Neural Information Processing Systems*, 2020.

- [73] A. Srinivas, M. Laskin, and P. Abbeel. Curl: Contrastive unsupervised representations for reinforcement learning. In *International Conference on Machine Learning*, 2020.
- [74] H. Liu and P. Abbeel. Behavior from the void: Unsupervised active pre-training. *arXiv preprint arXiv:2103.04551*, 2021.
- [75] D. Yarats, R. Fergus, A. Lazaric, and L. Pinto. Reinforcement learning with prototypical representations. In *International Conference on Machine Learning*, 2021.
- [76] S. Nair, A. Rajeswaran, V. Kumar, C. Finn, and A. Gupta. R3m: A universal visual representation for robot manipulation. *arXiv preprint arXiv:2203.12601*, 2022.
- [77] S. Parisi, A. Rajeswaran, S. Purushwalkam, and A. Gupta. The unsurprising effectiveness of pre-trained vision models for control. *arXiv preprint arXiv:2203.03580*, 2022.
- [78] D. Yarats, A. Zhang, I. Kostrikov, B. Amos, J. Pineau, and R. Fergus. Improving sample efficiency in model-free reinforcement learning from images. In *Proceedings of the AAAI Conference on Artificial Intelligence*, 2021.
- [79] E. Shelhamer, P. Mahmoudieh, M. Argus, and T. Darrell. Loss is its own reward: Self-supervision for reinforcement learning. *arXiv preprint arXiv:1612.07307*, 2016.
- [80] D. Yarats, R. Fergus, A. Lazaric, and L. Pinto. Mastering visual continuous control: Improved data-augmented reinforcement learning. *arXiv preprint arXiv:2107.09645*, 2021.
- [81] M. Laskin, K. Lee, A. Stooke, L. Pinto, P. Abbeel, and A. Srinivas. Reinforcement learning with augmented data. In *Advances in Neural Information Processing Systems*, 2020.
- [82] I. Kostrikov, D. Yarats, and R. Fergus. Image augmentation is all you need: Regularizing deep reinforcement learning from pixels. In *International Conference on Learning Representations*, 2021.
- [83] T. Xiao, I. Radosavovic, T. Darrell, and J. Malik. Masked visual pre-training for motor control. *arXiv preprint arXiv:2203.06173*, 2022.

Appendix

A Behavior Learning

We utilize the actor-critic learning scheme of DreamerV2 [15]. Specifically, we introduce a stochastic actor and a deterministic critic as below:

$$\text{Actor: } \hat{a}_t \sim p_\psi(\hat{a}_t | \hat{s}_t) \quad \text{Critic: } v_\xi(\hat{s}_t) \approx \mathbb{E}_{p_\theta} \left[\sum_{i \leq t} \gamma^{i-t} \hat{r}_i \right], \quad (8)$$

where $\{\hat{s}_t, \hat{a}_t, \hat{r}_t\}$ is imagined future states, actions, and rewards which are recursively obtained by conditioning on a initial state \hat{s}_0 and utilizing the transition model and the reward model in Equation 1, and the actor in Equation 8. Note that the initial state \hat{s}_0 is the model state obtained from the representation model in Equation 1 using the samples from the replay buffer. Then the critic is trained to regress the λ -target [42, 55] as follows:

$$\mathcal{L}^{\text{critic}}(\xi) \doteq \mathbb{E}_{p_\theta} \left[\sum_{t=1}^{H-1} \frac{1}{2} (v_\xi(\hat{s}_t) - \text{sg}(V_t^\lambda))^2 \right], \quad (9)$$

$$V_t^\lambda \doteq \hat{r}_t + \gamma \begin{cases} (1 - \lambda)v_\xi(\hat{s}_{t+1}) + \lambda V_{t+1}^\lambda & \text{if } t < H \\ v_\xi(\hat{s}_H) & \text{if } t = H, \end{cases} \quad (10)$$

where sg is a stop gradient function. Then we train the actor that maximizes the imagined return by back propagating the gradients through the learned world models as follows:

$$\mathcal{L}^{\text{actor}}(\psi) \doteq \mathbb{E}_{p_\theta} [-V_t^\lambda - \eta H[a_t | \hat{s}_t]], \quad (11)$$

where the entropy of actor $H[a_t | \hat{s}_t]$ is maximized to encourage exploration, and η is a hyperparameter that adjusts the strength of entropy regularization. We refer to Hafner et al. [15] for more details.

B Extended Qualitative Analysis

We provide our qualitative analysis in videos on our project website:

<https://sites.google.com/view/mwm-rl>

which contains videos for (i) reconstructions from masked autoencoders (MAE) [13] and (ii) predictions from latent dynamics models. To be self-contained, we also provide reconstructions from masked autoencoders with images in Appendix B.1.

B.1 Reconstructions from Masked Autoencoders

In this section, we provide motivating examples for introducing convolutional feature masking. Specifically, we provide reconstructions from MAE [13] trained on Coffee-Pull and Peg-Insert-Side tasks from Meta-world [16] in Figure 8. We find that reconstruction with pixel patch masking can be an extremely difficult objective, which makes it difficult for the model to learn the fine-grained details such as object positions. For instance, in Figure 8, MAE struggles to predict the position of objects (*e.g.*, a cup or a block) within masked patches, making it difficult to learn such details.

C Extended Related Work

Vision transformers with early convolution Introducing convolutional layers into a ViT architecture is not new. Dosovitskiy et al. [14] investigated a hybrid ViT architecture that utilizes a modified version of ResNet [56] to obtain a convolutional feature map. This has been followed by a series of works that investigate the architecture design to introduce convolutions for improved performance [45, 57]. While these works mostly consider deep convolutional networks to maximize the performance on downstream tasks, we introduce a lightweight convolution stem consisting of a few convolution layers, following the design of Xiao et al. [40]. This is because our motivation for introducing the convolution stem is to avoid the pitfall of reconstruction objective with masked pixel patches, but not to investigate the optimal hybrid ViT architecture that maximizes the performance.

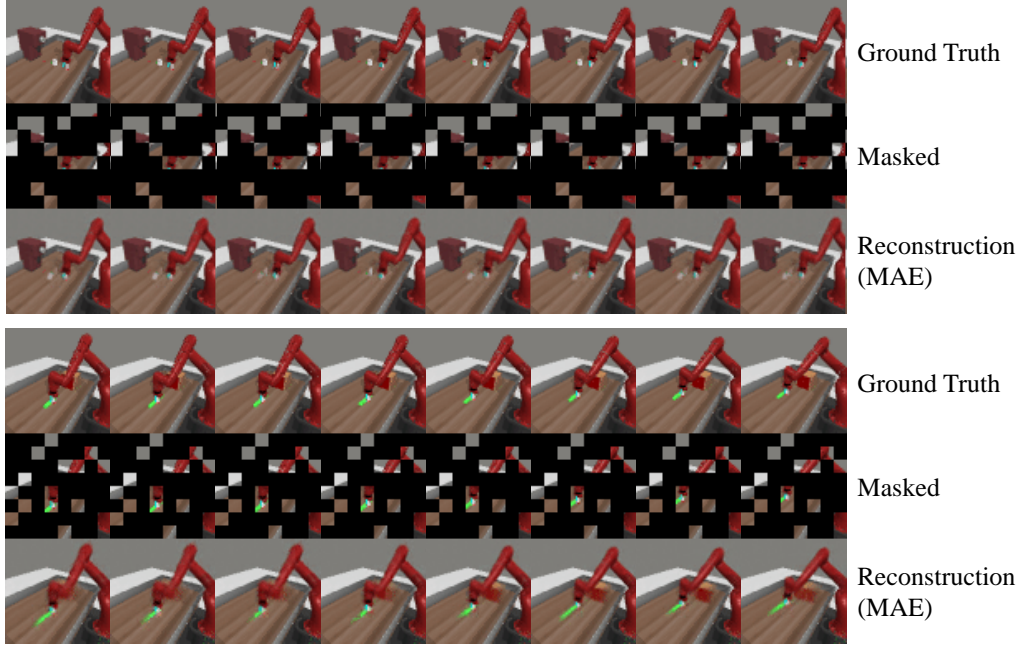


Figure 8: Frames reconstructed with the masked autoencoders (MAE) [13] trained on Meta-world (Top) Coffee Pull and (Bottom) Peg Insert Side. We find that reconstructions are not capturing the detailed object positions within patches. Best viewed as video provided in our website.

Convolutional feature masking In the context of semantic segmentation, Dai et al. [58] proposed to utilize convolutional feature masking instead of pixel masking. But this differs in that their goal is to utilize the masks as inputs to classifiers, unlike our approach that drops convolutional features with masks. More related to our work is the approaches that mask out convolutional features as a regularization technique [59, 60]. For instance, Tompson et al. [59] demonstrated that masking out entire channels for a specific feature from a convolutional feature map can be more effective than Dropout [61] that masks randomly sampled channels. Ghiasi et al. [60] further developed this idea by proposing DropBlock that masks contiguous region of a feature map. In the context of visual control, Park et al. [62] trained a VQ-VAE [63] and proposed to drop convolutional features corresponding to randomly sampled discrete latent codes. Our work extends the idea of masking out convolutional features to self-supervised learning with a ViT and demonstrates its effectiveness for representation learning in visual model-based RL.

Unsupervised representation learning for visual control Following the work of Jaderberg et al. [64] that demonstrated the effectiveness of auxiliary unsupervised objectives for RL, a variety of unsupervised learning objectives have been studied, including future latent reconstruction [27, 65, 66, 67], bisimulation [68, 69], contrastive learning [70, 71, 72, 73, 74, 30, 75, 29, 76, 77], world model learning [8, 9, 10, 54] and reconstruction [78, 79]. Recent approaches have also demonstrated that simple data augmentations can sometimes be effective even without such representation learning objectives [80, 81, 82]. The work closest to ours is Xiao et al. [83], which demonstrated that frozen representations from MAE pre-trained on real-world videos can be used for training RL agents on visual manipulation tasks. Our work differs in that we demonstrate that training a self-supervised ViT with reconstruction and convolutional feature masking can be more effective for visual control tasks when compared to MAE that masks pixel patches. We also note that our work is orthogonal to Xiao et al. [83] in that our framework can also initialize the autoencoder with pre-trained parameters.

D Pseudocode

For clarity, we define the optimization objectives for autoencoder and latent dynamics model, and describe the pseudocode for our method. Specifically, given a random batch $\{(o_j, r_j, a_j)\}_{j=1}^B$, visual representation learning and dynamics learning objectives are defined as:

$$\mathcal{L}^{\text{vis}}(\phi) = \frac{1}{B} \sum_{j=1}^B \left(-\ln p_{\phi}(o_j | z_j^{c,m}) - \ln p_{\phi}(r_j | z_j^{c,m}) \right) \quad (12)$$

$$\begin{aligned} \mathcal{L}^{\text{dyn}}(\theta) = \frac{1}{B} \sum_{j=1}^B \left(-\ln p_{\theta}(z_j^{c,0} | s_j) - \ln p_{\theta}(r_j | s_j) \right. \\ \left. + \beta \text{KL} \left[q_{\theta}(s_j | s_{j-1}, a_{j-1}, z_j^{c,0}) \parallel p_{\theta}(\hat{s}_j | s_{j-1}, a_{j-1}) \right] \right) \end{aligned} \quad (13)$$

Algorithm 1 Masked World Models

- 1: Initialize parameters of autoencoder ϕ , latent dynamics model θ , actor ψ , and critic ξ
 - 2: Initialize replay buffer $\mathcal{B} \leftarrow \emptyset$
 - 3: **for** each timestep t **do**
 - 4: // COLLECT TRANSITIONS
 - 5: Get autoencoder representation $z_t^{c,0}$
 - 6: Update model state $s_t \sim q_{\theta}(s_t | s_{t-1}, a_{t-1}, z_t^{c,0})$
 - 7: Sample action $a_t \sim p_{\psi}(a_t | s_t)$
 - 8: Add transition to replay buffer $\mathcal{B} \leftarrow \mathcal{B} \cup \{(o_t, a_t, r_t)\}$
 - 9: // VISUAL REPRESENTATION LEARNING WITH REWARD PREDICTION
 - 10: Sample random minibatch $\{(o, r)\} \sim \mathcal{B}$
 - 11: Update autoencoder by minimizing $\mathcal{L}^{\text{vis}}(\phi)$
 - 12: // DYNAMICS LEARNING
 - 13: Sample random minibatch $\{(o, r, a)\} \sim \mathcal{B}$
 - 14: Update latent dynamics model by minimizing $\mathcal{L}^{\text{dyn}}(\theta)$ and obtain states $\{s\}$
 - 15: // ACTOR CRITIC LEARNING
 - 16: Imagine future rollouts $\{\hat{s}, \hat{a}, \hat{r}\}$ from $\{s\}$ using latent dynamics model and actor
 - 17: Update actor by minimizing $\mathcal{L}^{\text{actor}}(\psi)$
 - 18: Update critic by minimizing $\mathcal{L}^{\text{critic}}(\xi)$
 - 19: **end for**
-

E Architecture Details

E.1 Autoencoder

Convolution stem and masking We use visual observations of $64 \times 64 \times 3$. For the convolution stem, similar to the design of Xiao et al. [40], we stack 3 convolution layers with the kernel size of 4×4 and stride 2, followed by a convolution layer with the kernel size of 1×1 . This convolution stem processes o_t into $8 \times 8 \times 256$, which has the same spatial shape of 8×8 when we use the patchify stem with patch size of 8×8 . Then a masking is applied with a masking ratio of $m = 0.75$.

ViT encoder and decoder We use a 4-layer ViT encoder and a 3-layer ViT decoder, which are implemented using `tfimm`³ library. The ViT encoder concatenates class token with un-masked convolutional features, embeds inputs into 256-dimensional vectors, and processes them through Transformer layers. Then the ViT decoder takes outputs from the encoder and concatenate learnable mask tokens into them. Here, we use the same learnable mask token for reward prediction, which can be discriminated from other mask tokens because it gets different positional encoding. Finally, two linear output heads for predicting pixels and rewards are used to generate predictions. Unlike MAE, we compute the loss on entire pixels because we do not apply masking to pixels.

³<https://github.com/martinsbrucheris/tensorflow-image-models>

Initialization with warm-up schedule We initialize parameters of the autoencoder using 5000 gradients steps with a linear warm-up schedule over initial 2500 steps using the samples collected from initial random exploration. We find this improves sample-efficiency on relatively easy tasks, but does not make significant difference on complex tasks. This is because better visual representations are used for learning latent dynamics models from the beginning. However, we also observe that this initialization is not required when we update the parameters in a more short interval (*e.g.*, every 2 timesteps instead of 5 timesteps), because the autoencoder can be trained quickly without introducing such an initialization period. In our experiments, we use the initialization scheme and update the parameters every 5 timesteps for faster experimentation.

E.2 Latent Dynamics Model

Architecture Our model is built upon the discrete latent dynamics model introduced in DreamerV2. Inputs to our model are representations $z_t^{c,0}$ from the autoencoder, which are of shape $8 \times 8 \times 256$ obtained by processing the visual observations through the convolution stem and ViT encoder of our autoencoder without masking (*i.e.*, $m = 0$). Because our dynamics model does not take visual observations as inputs, we do not utilize CNN encoder and decoder as in the original architecture. Instead, we introduce a shallow 2-layer ViT encoder and decoder with the embedding size of 128, which takes $z_t^{c,0}$ as inputs. Following Seo et al. [54], we increase the hidden size of dense layers and the model state dimension from 200 to 1024.

Prediction visualization While the latent dynamics model is not trained directly to reconstruct raw pixels, its predictions can still be used for visualizing the open-loop predictions. This is because it is trained to reconstruct $z_t^{c,0}$, which can be processed through the ViT decoder of the autoencoder. We use this scheme for visualizing the predictions from the model in Figure 7.

F Experiments Details

Meta-world experiments In order to use a single camera viewpoint consistently over all 50 tasks, we use the modified corner2 camera viewpoint for all tasks. Specifically, we adjusted the camera position with `env.model.cam_pos[2][:] = [0.75, 0.075, 0.7]`, rendering visual observations as in Figure 2 which enables us to solve non-zero success rate on all tasks. Maximum episode length for Meta-world tasks is 500. We use the action repeat of 2, which we find it easy to solve tasks compared to the action repeat of 1 used in Seo et al. [54].

In our experiments, we classify 50 tasks into easy, medium, hard, and very hard tasks where experiments are run over 500K, 1M, 2M, 3M environments steps with action repeat of 2, respectively.

Difficulty	Tasks
easy	Button Press, Button Press Topdown, Button Press Topdown Wall, Button Press Wall, Coffee Button, Dial Turn, Door Close, Door Lock, Door Open, Door Unlock, Drawer Close, Drawer Open, Faucet Close, Faucet Open, Handle Press, Handle Press Side, Handle Pull, Handle Pull Side, Lever Pull, Plate Slide, Plate Slide Back, Plate Slide Back Side, Plate Slide Side, Reach, Reach Wall, Window Close, Window Open, Peg Unplug Side
medium	Basketball, Bin Picking, Box Close, Coffee Pull, Coffee Push, Hammer, Peg Insert Side, Push Wall, Soccer, Sweep, Sweep Into
hard	Assembly, Hand Insert, Pick Out of Hole, Pick Place, Push, Push Back
very hard	Shelf Place, Disassemble, Stick Pull, Stick Push, Pick Place Wall

RLBench experiments We consider two relatively easy tasks (*i.e.*, Reach Target and Push Button) with dense rewards, and utilize an action mode that specifies the delta of joint positions. Because original RLBench repository does not support shaped rewards for Push Button task, we design a shaped rewards for Push Button following the design of rewards in Reach Target. Specifically, the reward is defined as the sum of (i) the L2 distance of gripper to a button and (ii) the magnitude of the button being pushed. We set the maximum episode length to 200, and use the action repeat of 2. Because RLBench is designed to be episodic unlike Meta-world, we use the discount prediction

scheme in DreamerV2 that introduces a linear head that predicts the termination of each rollout. For visual observations, we use the front RGB observation (see Figure 2 for an example).

DeepMind Control Suite experiments We follow the setup of Hafner et al. [21] where the action repeat of 2 is used. We use default camera configurations without modification. We note that direct comparison with the results from Hafner et al. [21] is not possible because our experiments are based on DreamerV2 with larger networks (see Appendix E.2 for architecture details).

Computation In terms of parameter counts, MWM consists of 25.9M parameters while DreamerV2 consists of 33.2M parameters. However, in terms of training time, MWM takes 5.5 hours for training over 500K environment steps, which is 1.57 times slower than DreamerV2 that takes 3.5 hours, because MWM processes visual observations through low-throughput ViT twice with and without masking. Given the improvement in final performances and sample-efficiency on complex tasks as demonstrated in our experiments, we note that it is worth spending additional computational costs.

Hyperparameters We report the hyperparameters used in our experiments in Table 1.

Table 1: Hyperparameters used in our experiments. Unless otherwise specified, we use the same hyperparameters used in DreamerV2 [15]. DMC is an abbreviation of DeepMind Control Suite.

Hyperparameter	Value
Image observation	$64 \times 64 \times 3$
Image normalization	Mean: (0.485, 0.456, 0.406), Std: (0.229, 0.224, 0.225)
Action repeat	2
Max episode length	500 (Meta-world), 200 (RLBench), 1000 (DMC)
Early episode termination	True (RLBench), False otherwise
Random exploration	5000 environment steps
Reward normalization	False (DMC), True otherwise
World model batch size	16 (DMC), 50 otherwise
World model sequence length	50
World model tradeoff (β)	0.1 (RLBench), 1.0 otherwise
World model tradeoff free-bits	0.1 (RLBench), 0.01 otherwise
World model ViT encoder size	2 layers, 4 heads, 128 units
World model ViT decoder size	2 layers, 4 heads, 128 units
Autoencoder batch size	1024
Autoencoder initialization steps	5000
Autoencoder warm-up steps	2500
Autoencoder learning rate	$3 \cdot 10^{-4}$
Autoencoder masking ratio	0.75
Autoencoder ViT encoder size	4 layers, 4 heads, 256 units
Autoencoder ViT decoder size	3 layers, 4 heads, 256 units

G Full Meta-world Experiments

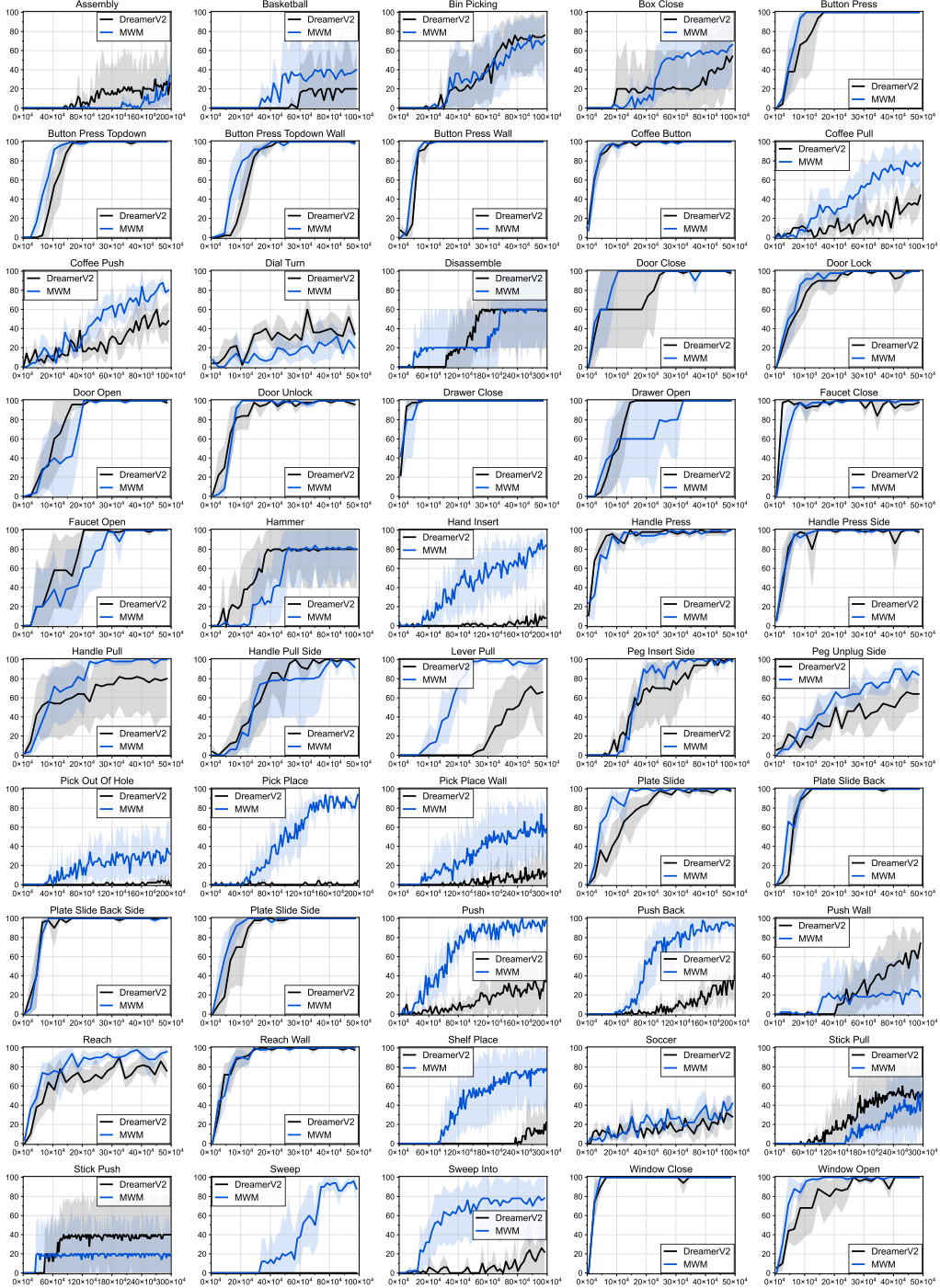


Figure 9: Learning curves on 50 visual robotic manipulation tasks from Meta-world as measured on the success rate. The solid line and shaded regions represent the mean and bootstrap confidence intervals, respectively, across five runs.

H Additional DeepMind Control Suite Experiments

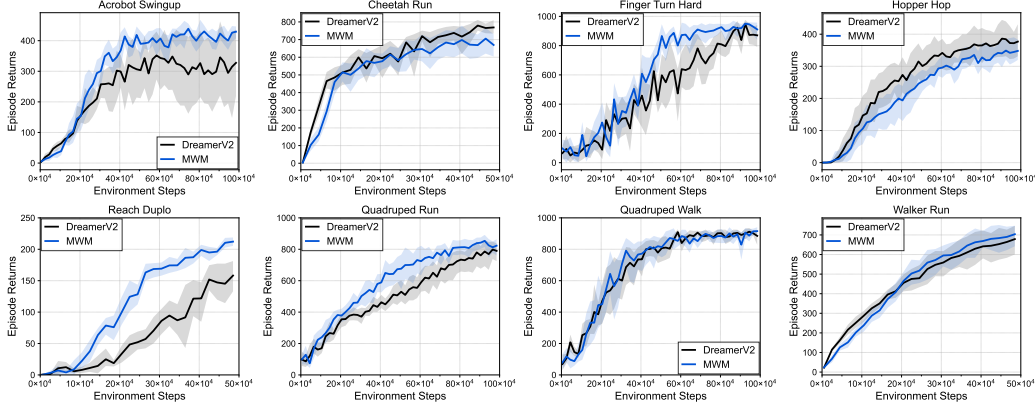


Figure 10: Learning curves on eight visual robot tasks from DeepMind Control Suite as measured on the episode return. The solid line and shaded regions represent the mean and bootstrap confidence intervals, respectively, across eight runs.

I Extended Ablation Study and Analysis

We provide additional analysis in Figure 11 and learning curves on individual tasks in Figure 12.

Utilizing only CLS representation We ablate our design choice of utilizing all representations of $z_t^{c,0}$ for dynamics learning, instead of using only CLS representation as in MAE. As shown in Figure 11(a), we find that utilizing all representations (*i.e.*, CLS + Conv) outperforms the baseline (*i.e.*, CLS), by encouraging the model to learn spatial information included in all representations.

Model size We report the performance of our method with varying number of layers for autoencoders in Figure 11(b). We find that there are no significant differences between three models sizes we consider, which might be because Meta-world visual observations are not too complex. It would be interesting to investigate the effect of model sizes in more complex environments.

DreamerV2 with ViT In order to demonstrate that performance gain from our approach does not solely come from employing ViT instead of CNN, we evaluate DreamerV2 w/ ViT that replaces CNN encoder and decoder with ViT encoder and decoder, in Figure 11(c). We find DreamerV2 w/ ViT exhibits severe instability during training, and sometimes becomes completely unable to solve the tasks. We conjecture this might be because ViT suffers from unstable training without large data and regularization [14], which makes it difficult to learn world models end-to-end.

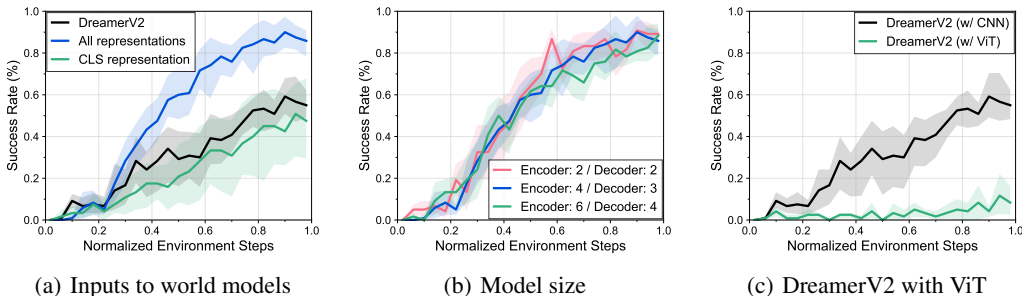


Figure 11: Learning curves on three manipulation tasks from Meta-world that investigate the effect of (a) inputs to world models and (b) autoencoder model sizes. (c) We also report the performance of DreamerV2 with CNNs and ViT. The solid line and shaded regions represent the mean and stratified bootstrap confidence interval across 12 runs.

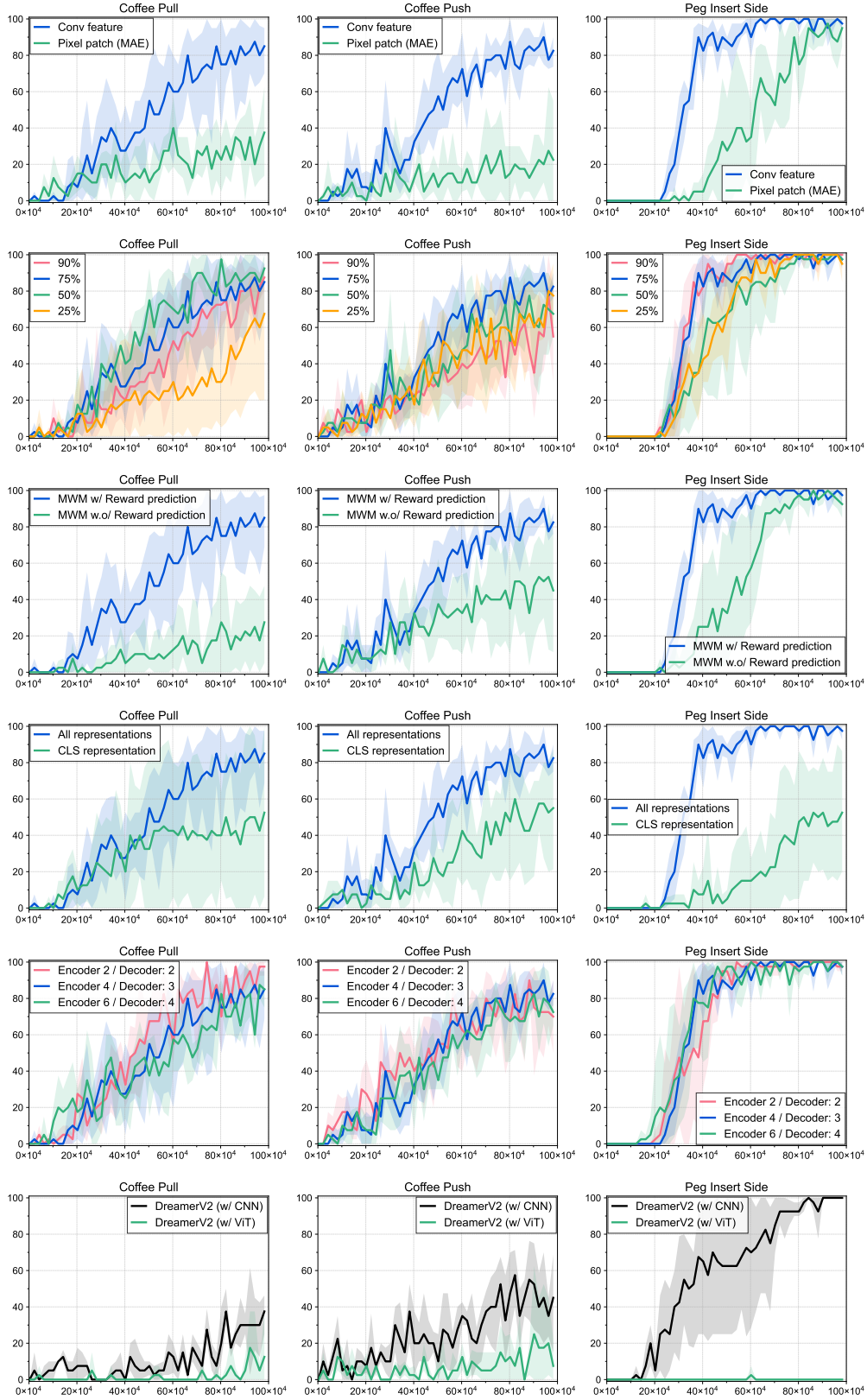


Figure 12: Learning curves on individual tasks used in ablation studies and analysis. The solid line and shaded regions represent the mean and bootstrap confidence interval across 4 runs.